

Fast Ion Physics from Neutral Particle Analysis on the Large Helical Device

LYON James F.* and SPONG Donald A.
Oak Ridge National Laboratory, Oak Ridge, TN 37831-8072, USA

(Received: 30 September 1997/Accepted: 12 February 1998)

Abstract

Time-resolved measurements of the energetic ion distribution from different viewing angles allow study of some important aspects of stellarator physics. Examples from the Advanced Toroidal Facility (ATF) of measurements of the ion distribution function and the variation of orbits with pitch v_i/v and electric field are used to illustrate some of these points; ATF's magnetic configuration was similar to that of the Large Helical Device (LHD). Silicon ion-implanted detectors should allow measurements of the ion distribution function that are difficult with conventional neutral particle analyzers (NPAs) on LHD. Application of a silicon-detector NPA array on LHD is discussed.

Keywords:

fast ion distribution, neutral particle analyzer, charge-exchange measurements, particle orbits, stellarator/heliotron, Large Helical Device

1. Energetic Ion Distributions and Related Physics

Some important aspects of stellarator/heliotron physics can be studied best from time-resolved charge-exchange measurements of the energetic ion distribution in energy, space, and pitch angle. The complexities arising from the different orbit classes and the full three-dimensional magnetic field geometry necessitate measurements and modeling of the charge-exchange flux along different viewing lines.

Charge-exchange measurements of the fast ion distribution from neutral beam injection (NBI) give information on loss regions, Z_{eff} , the electron temperature T_e , the ratio of loss times to slowing down times, and other plasma properties when compared with Fokker-Planck modeling of the NBI-created fast ions as they slow down in energy and scatter in pitch angle on the background thermal plasma [1]. Similarly, measurements of the fast ion distribution created by ion cyclotron range of frequency (ICRF) heating give information on the energetic-particle loss regions, the ion-

minority fraction, etc. Figure 1 [2] shows the charge-exchange flux from ICRF heating in ATF obtained by an NPA scanning toroidally (in pitch, or v_i/v). Near-perpendicular heating and a low- v_i/v loss region at higher energy can be seen in the data. In addition, measurements of the charge-exchange spectrum allow study of the physics derived from the thermal ion distribution: ion heating, ion heat diffusivity, ion rotation velocity, transport barriers, etc.

2. Energetic Ion Orbits

Guiding-center orbit calculations can be used to indicate the type of fast ion behavior expected in LHD. Figures 2–4 are plots in flux coordinates of H^+ orbits with energy $W = 1$ keV launched at half the plasma radius ($r/a = 0.5$) on the outside midplane with v_i/v ranging from 0 to +1 (co-direction) or -1 (counter-direction). The magnetic configuration is similar to that of ATF and LHD but with major radius $R_0 = 1$ m and magnetic field $B_0 = 1$ T. These cases correspond to 52

*Corresponding author's e-mail: lyonjf@fed.ornl.gov

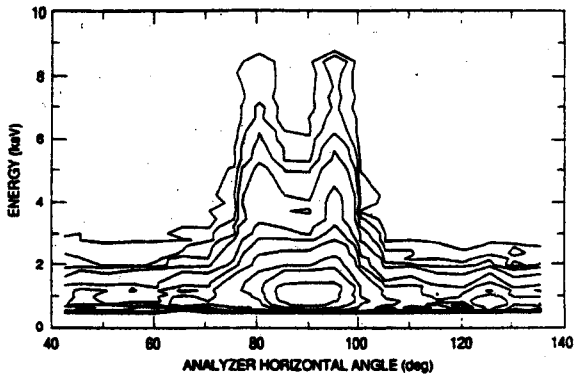


Fig. 1 Contours of constant H^0 charge-exchange flux obtained during H-minority ICRF heating in ATF for a horizontal midplane scan.

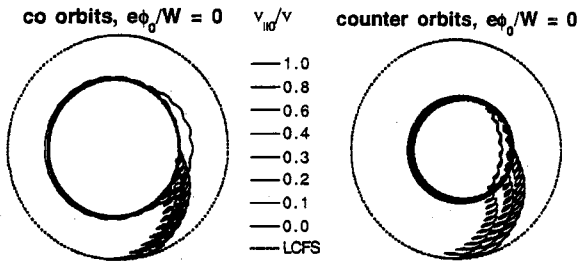


Fig. 2 Co and counter 1 keV H^+ orbits in ATF with no electric field.

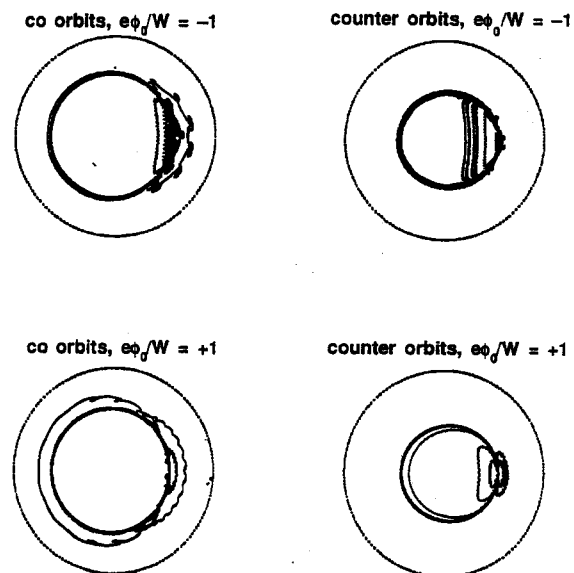


Fig. 3 Co and counter 1 keV H^+ orbits in ATF with $\phi_0 = \pm 1$.

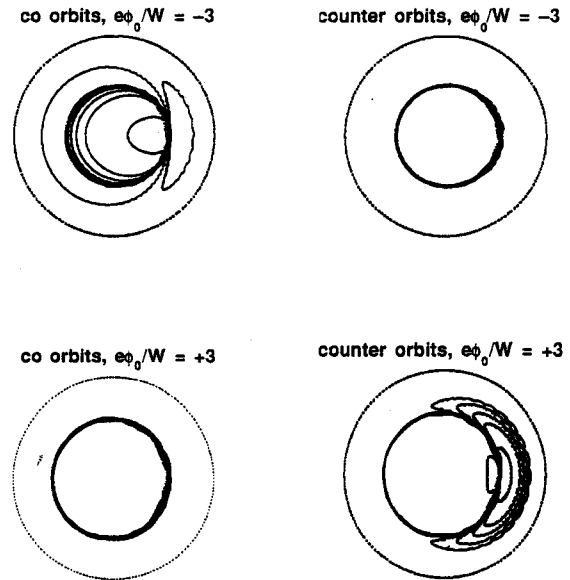


Fig. 4 Co and counter 1 keV H^+ orbits in ATF with $\phi_0 = \pm 3$.

keV H^+ orbits or 26 keV D^+ orbits for $B_0 = 3$ T in LHD. A Gaussian potential profile, $\phi = \phi_0 \exp[-(r/a)^2]$, is assumed in these calculations.

Figure 2 shows “co” and “counter” orbits for no electric field. Helically trapped orbits are lost for $|v_{||}/v| \leq 0.2$. The co orbits drift outside their birth flux surface, and the counter orbits drift inside. Figure 3 shows the effect on co and counter orbits of a radial electric field E with $\phi_0/W = \pm 1$. The $E \times B$ drift overcomes the unfavorable $B \times \nabla B$ drift of the helically trapped particles, and the orbits are no longer lost. The counter particles are better confined because the orbit deviations are inside their birth flux surface. Figure 4 shows the effect on co and counter orbits of a radial electric field with $\phi_0/W = \pm 3$. All co orbits for $\phi_0/W = +3$ and counter orbits for $\phi_0/W = -3$ are well confined. However, orbit confinement becomes worse for co orbits for $\phi_0/W = -3$ and for counter orbits for $\phi_0/W = +3$ because the $E \times B$ drift resonates with the parallel particle drift. Little improvement is seen for $\phi_0/W = \pm 5$, but good confinement is restored by $\phi_0/W = \pm 10$. The effect of the lost orbits should appear as a dip in the charge-exchange spectrum at $W > 3T_e$ for near-perpendicular particles (see Fig. 1) and at $W \sim (0.5-1)T_e$ for passing particles because ϕ_0 should be $\sim (2-3)T_e$.

Nearly the same orbits are obtained at 10 keV for the same value of ϕ_0/W . The orbits are more chaotic (the structure seen in Fig. 4 disappears), but the deviations from a flux surface are approximately the same as

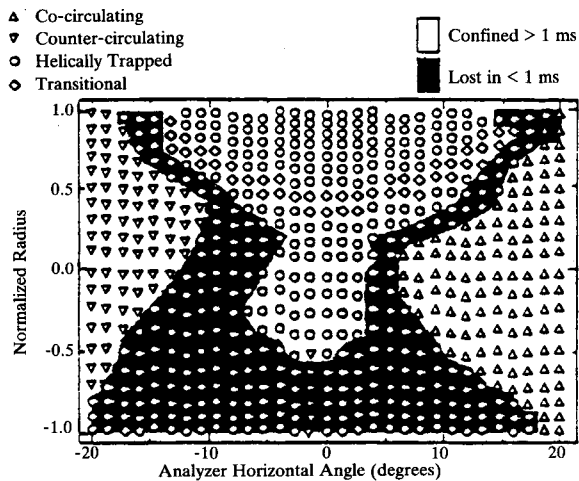


Fig. 5 Confined and loss regions and the orbit types for 10 keV H^+ with no electric field as seen by the toroidally scanning ATF NPA in the equatorial plane at $B_0 = 1$ T.

for $W = 1$ keV. Figure 5 shows the calculated confined and loss regions and the orbit types for 10 keV H^+ with no electric field as seen by an NPA scanning toroidally in the equatorial plane in ATF at $B_0 = 1$ T. Helically trapped particles are lost on the outside of the torus (negative radius) and confined on the inside of the torus (positive radius). Both co and counter passing particle orbits are confined.

3. Neutral Particle Analyzers

Standard NPAs use electric and magnetic fields to sort charge-exchange neutral particles into a small number of energy channels after the charge-exchange neutrals have been ionized in a gas stripping cell. These NPAs are typically very large (~ 300 - to 600 -kg) instruments that need to be placed far enough from an experiment to avoid creating magnetic field perturbations which produce islands that affect plasma performance. This and their large size and cost limit their number.

Silicon detectors [3] offer another approach at the ion energies expected in LHD. Neutral particles (a stripping cell is not needed) incident on a detector create an electron-hole pair in the depleted volume in the silicon for each 3.62 eV of particle energy, producing a charge pulse proportional to the energy of the incident particle. These instruments are small, (typically ~ 5 cm) and relatively inexpensive, use no iron or magnetic field (so no field perturbation is created), and can operate in vacuum and in high magnetic fields. These properties permit their use in compact arrays for simultaneous

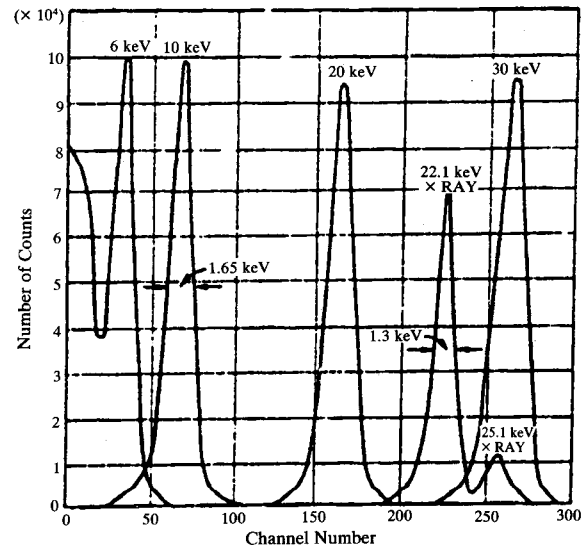


Fig. 6 Pulse height distributions obtained with a 50 mm^2 silicon surface barrier detector [4].

charge-exchange measurements along multiple viewing chords, similar to the use of silicon detectors in soft X-ray diode arrays.

The detector and the front end of a close-coupled charge-sensitive preamplifier are cooled with liquid nitrogen to produce low noise and good energy resolution, ≈ 1.7 keV from ~ 5 keV to 8 MeV (for a $500\text{-}\mu$ depletion depth). Figure 6 [4] shows the results for H^0 particles at 6, 10, 20, and 30 keV and 22.1- and 25.1 keV X-rays from ^{109}Cd for a 50 mm^2 silicon surface barrier detector (800 \AA dead layer). A 6 keV H^0 peak is distinguishable from the background. This type of detector was routinely used in the mid-1960s to measure the radial and pitch-angle distribution of energetic ions in the DCX-2 mirror experiment [5].

4. Application to LHD

LHD will have a time-of-flight NPA, and the ATF *EllB* NPA is also being considered. These are large instruments that can be moved from shot to shot to give an angular scan of the charge-exchange flux from the plasma. A compact silicon detector NPA array is also proposed.

Ion-implanted silicon detectors [6] have a thin (500 \AA) front electrode. A thin (800 \AA) aluminum coating can be applied to the front surface to make the detectors insensitive to light from the plasma. Minimizing the thickness of this dead layer is important in reducing the lowest energy that can be measured. The

range of H^0 in silicon is 500 Å at 3 keV and 1000 Å at 7 keV. Both the detectors and the front end of the close coupled (to minimize capacitance) preamplifiers are cooled below -60°C to reduce the leakage current and improve the energy resolution (1.6 keV cooled and 3.3 keV at room temperature). It should be possible to detect H^0 for $W > 7-10$ keV with the aluminum coating. In addition to measurements of the energetic ion spectrum from NBI and ICRF heating, this detector should allow determination of ion temperatures $T_i > 1$ keV because T_i is determined from the charge-exchange flux in the energy range $W = (7-10) T_i$ for a perpendicular passive measurement.

The proposed NPA design features a collimating slit and a linear array of six silicon detectors. The six-detector array provides simultaneous measurements along different lines of sight in one dimension; the slit is moved from shot to shot to provide a scan in the orthogonal direction for a full two-dimensional scan of the plasma, similar to the four-detector soft-X-ray system on LHD. X-ray and α -particle sources would also be mounted on the shaft that changes the pinhole size for *in-situ* calibration and energy resolution measurements. The proposed location is on the horizontal midplane in the same port as the time-of-flight NPA, which would allow comparisons with it for both horizontal and vertical viewing lines.

Up to 4096 256-channel pulse height spectra, one every 3–10 ms, can be measured for each shot for each detector and the data stored for later analysis and modeling. One of three different-size pinholes can be selected to keep the count rate $\leq 100,000 \text{ s}^{-1}$. Since

pulse height analysis is used, the only source of "noise" is visible and uv light from the plasma. This produces a low-pulse-height background (seen in Fig. 6), which is easily accounted for, and decreased energy resolution. Extensive baffling and low-reflectance surfaces (anodized aluminum) can be used to minimize this problem, in addition to the thin (800 Å) aluminum coating on the surface of the detectors discussed earlier.

Acknowledgments

The authors acknowledge discussions with S. Sudo, T. Ozaki, A. Hyder, M. Martini, B. Nelson, J. Rome, P. Sangsingkeow and W. Tucker. This work was supported by the Office of Fusion Energy Sciences, U.S. Department of Energy, under Contract No. DE-AC05-96OR22464 with Lockheed Martin Energy Research Corp.

References

- [1] *Thermonuclear Div. Ann. Progr. Rept.* Dec. 31, 1974, ORNL-5053, p.11.
- [2] M. R. Wade *et al.*, *Rev. Sci. Instrum.* **61**, 3202 (1990).
- [3] F. S. Goulding and R.H. Pehl, *Semiconductor Detectors*, Section IIIA, Academic Press (1974).
- [4] J. A. Ray and C. F. Barnett, *IEEE Trans. Nucl. Sci.*, NS **16**, 82 (1969).
- [5] *Thermonuclear Div. Semiann. Progr. Rept.* Oct. 31, 1966, ORNL-4063, sect. 2.4.
- [6] *Modular Pulse-Processing Electronics and Semiconductor Radiation Detectors*, EG&G ORTEC, Inc., 1997.